On chip MnO2-based 3D micro-supercapacitors with ultra-high areal energy density

Botayna Bounor, Bouchra Asbani, Camille Douard, Frédéric Favier, Thierry Brousse, Christophe Lethien

On chip MnO_2-based 3D micro-supercapacitors with ultra-high areal energy density

Botayna Bounor[1,2] Bouchra Asbani[1,2] Camille Douard[3] Frederic Favier[4]

Thierry Brousse[2,3] Christophe Lethien[1,5,2]

[1]IEMN - Institut d'Électronique, de Microélectronique et de Nanotechnologie (IEMN) - UMR 8520

[2]RS2E - Réseau sur le stockage électrochimique de l'énergie

[3]IMN - Institut des Matériaux Jean Rouxel

[4]ICGM ICMMM - Institut Charles Gerhardt Montpellier - Institut de Chimie Moléculaire et des Matériaux de Montpellier

[5]CSAM - IEMN - Circuits Systèmes Applications des Micro-ondes - IEMN

Abstract

In the near future, Internet of Things will be widely deployed all over the connected world. Powering will be crucial for miniaturized electronic devices requiring fast charging, high energy density and long term-durability. 3D micro-supercapacitors are an attractive energy storage solution at the millimeter scale to power miniaturized IoT devices exhibiting small form factor packaging issues. However, there are nowadays not any microdevices on the shelves that could fulfill both energy and mass production requirements. Here, we demonstrate the collective fabrication of 3D micro-supercapacitors (MSCs) integrated on silicon wafer and using MnO_2 as the active electrode material and 5M aqueous $LiNO_3$ as the electrolyte. 0.05 – 0.1 mWh cm^{-2} energy densities reached by the fabricated 3D MSCs are remarkable, exceeding those of state-of-the-art micro-supercapacitors, competing those of hybrid microdevices and approaching the performance of lithium micro-batteries. Without sacrificing the power performance (> 1 mW cm^{-2}), the 3D MSCs demonstrate a very good cycling behavior over 10 000 cycles (~ 15 % loss).

Introduction

Autonomy is a key parameter to power nomadic Internet of Things (IoT) devices [1]. Energy storage systems able to deliver significant energy densities at high charge / discharge rates remain sought for the next generation of IoT networks for health, environmental or industrial monitoring, drug delivery (*in vivo* application), transportation, wearable personal electronics, and smart buildings [2]. Micro-supercapacitors (MSCs) [3–5] are widely investigated for such purpose. However, limited footprint surface of MSCs is required since advanced small form factor packaging methods such as 3D System-in-Package (3D SiP) technology integrate many electronic functions including the miniaturized energy harvesting and storage sources. This, in turn, limits the amount of active material and the stored energy.

Among all the materials considered for MSC electrodes, different forms of carbon have been envisioned. They store charges in the double layer at the electrode / electrolyte interface via the electrosorption of ions in the pores: the corresponding energy density is limited but the fast electrostatic storage process leads to high power microdevices [3,5]. Alternatively, pseudocapacitive materials can be used as electrodes for MSCs. For this class of electroactive compounds, the charge storage mechanism involves fast and reversible redox reactions occurring at the surface and subsurface of the material [6–9] thus conferring to the electrode a capacitive-like signature. Pseudocapacitive electrodes can exhibit greater capacitances than nanoporous carbon electrodes owing to the charge transfer that occur at the surface of the electrodes, while keeping fast charge / discharge rates thanks to these surface redox reactions.

Numerous pseudocapacitive materials such as 2D Transition Metal Carbides (MXene) [10–12], Transition Metal Nitrides (TMN: Mo_xN, VN…) [9,13–16], or

Transition Metal Oxides (TMO: RuO_2, MnO_2, T-Nb_2O_5) [17–21] have been investigated for on chip micro-supercapacitors. The most straightforward solution to improve the energy performance of miniaturized electrochemical capacitors deals with the deposition of thick electrodes using these pseudocapacitive materials [2]. Micro-supercapacitors with 200 µm-thick activated carbon [22] electrodes or 16 µm-thick pseudocapacitive vanadium nitride [16] films successfully demonstrated high energy density performance while keeping high the power density. A hybrid miniaturized device (footprint surface = 0.714 cm^2) was recently published by O. Schmidt *et al* [23]. A capacitive electrode (carbon nanotube) and a faradic one ($Cu_{0.56}Co_{2.44}O_4$@MnO_2) were combined in an interdigitated configuration based on Ti/Au current collectors. A PVA / KOH gel electrolyte packages the miniaturized device which deliver a very high energy density (0.18 $mWh.cm^{-2}$) owing to very thick bulk electrodes made from slurry (~ 0.4 mm-thick).

Another attractive solution to significantly enhance the energy density of MSCs while keeping low the thickness of TMO electrode is to increase the electrode surface. To limit the detrimental effect of enlarged electrode surfaces on the device footprint, 3D electrodes have become an attractive opportunity. They allow to maximize the surface contact between the electrode material and the electrolyte thanks to the increase of the area enhancement factor (AEF) of a 3D scaffold. Indeed, thin film deposition on high AEF 3D scaffolds increases the mass loading of active material, thus allowing to reach remarkable areal capacitance values [7,8,24–26]. Nevertheless, the proposed technology used to fabricate the 3D scaffold must also be compatible with semiconductor fabrication processes to favor a rapid scale-up of the technology towards pilot production line for mass production. Collective fabrication methods [3,8,9,24,27,28] aiming at producing numerous robust 3D

scaffolds with the same AEF per silicon wafer and no variation of the geometrical parameters have to be selected to improve the technological readiness level of this technology.

Here, we demonstrate the collective fabrication of high performance on chip 3D micro-supercapacitors using processes fully compatible with those currently used in microelectronics. Parallel plate or interdigitated configurations were achieved, using MnO_2 thin film as active material. In order to evaluate the performance of the fabricated 3D MSCs, 5M $LiNO_3$ aqueous electrolyte has been used although the final goal is to implement gel-type or solid-state electrolytes in our miniaturized electrochemical capacitors. $LiNO_3$ was chosen because of its higher solubility limit at room temperature thus higher ionic conductivity compared to sulfate based lithium or sodium salts, its wider operating temperature range and an increase in the capacitance of MnO_2 with this electrolyte compared to Na_2SO_4 [29,30]. Energy densities reached by the fabricated 3D MSCs (0.05 – 0.1 mWh cm^{-2}) are remarkable, exceeding those of state-of-the-art micro-supercapacitors (~ 0.001 – 0.03 mWh cm^{-2}) and competing that of the Zn-ion microdevice [31]. 3D MSCs (1V cell voltage) demonstrate a very good cycling behavior over 10 000 cycles (~ 15 % loss). Additionally, the low thickness of the MnO_2 films (< 1 µm) facilitates not only the rapid diffusion of ions but also fast electron transport in the electrode. The areal capacitance (~ 1.5 F cm^{-2}) of the fabricated 3D electrodes competes with that of classical bulk EC electrodes thanks to the conformal deposition of MnO_2 films on 3D scaffolds exhibiting high area enhancement factor (AEF). We show in the present paper, how the tuning of the MSC configuration, the thickness of the electrode material and the AEF of the 3D scaffold allow to reach more than 0.1 mWh cm^{-2}

energy density without sacrificing neither the power density (> 1 mW cm^{-2}) nor the cycling performance (>10 000 cycles).

Methods

Fabrication of the 3D electrodes. The technological process, illustrated in **figure S1** and allowing the fabrication of the 3D electrodes, is compatible with the microfabrication methods available in the semiconductor industry. Spin coating of a photoresist (SPR 220) is achieved on a (100) 3'' silicon wafer. A photolithography step is then applied to define the pattern. The silicon wafer is processed to fabricate the 3D scaffold. The silicon microtubes are fabricated using the Bosch dry etching process. The opened structure of these microtubes allows the deposition of active material both in the outside surface of the tubes but also in the inside surface. Subsequently, high aspect ratio Si microtubes are obtained and the etched depth is tuned with the number of Bosch cycles.

From the geometric dimensions of the silicon microtubes scaffold (**figure 1A**), the area enhancement factor (AEF) of the template can be calculated using the following formula (1):

$$AEF = 1 + \frac{(P_{IN} \times d_{IN} + P_{OUT} \times d_{OUT})}{pitch^2} \qquad (1)$$

where P_{IN} is the inner perimeter of the square shape silicon microtubes (4 x 3 µm), P_{OUT} is the outer perimeter of the microtube (4 x 6 µm), d_{OUT} is the etched depth of the electrode and $d_{IN} = \frac{d_{OUT}}{2}$(internal depth of the Si microtube). The structure pitch (pitch parameter = 9 µm) corresponds to the sum of the spacing between microtubes and the outer diameter of the Si microtube.

An Al_2O_3 layer (50 nm-thick) and a Pt film (50 nm-thick) are then conformally deposited by Atomic Layer Deposition to fabricate a 3D metallic current collector. On the one hand, the Al_2O_3 layer acts as insulating film allowing the fabrication of

numerous MSCs on a single silicon wafer without any electrical contact between those microdevices. This layer also prevents the chemical etching or dissolution of the silicon wafer regarding the aqueous solution used for electrochemical operation. On the other hand, Pt layer is considered as an efficient metallic current collector for the MSCs.

The Al_2O_3 layer was deposited by ALD using a Beneq TFS200 reactor which is a hot wall, flow through type reaction chamber operating in thermal ALD mode. The deposition temperature range was set to 300 °C. A Trimethylaluminium (TMA) served as the precursor and H_2O as the reactant (second precursor) to achieve the deposition of step conformal Al_2O_3 layer (50 nm-thick) on 3D scaffold. A platinum current collector (thickness: 50 nm) was also deposited by ALD using the same Beneq TFS200 tool. The precursors used for the deposition of platinum films by ALD were Trimetyl(methylCyclopentadienyl)Platinum ($MeCpPtMe_3$) and H_2O. The two self-limiting surface reactions that define Pt ALD growth are :

1. $MeCpPtMe_3$ adsorption

2. $MeCpPtMe_3$ ads + $H_2O \rightarrow Pt + CO_{2(g)} + H_{2(g)} + CH_{4(g)}$

The platinum precursor canister was heated at 54 °C while the substrate holder was kept at 300 °C.

The first reaction step consists of the introduction of MeCpPtMe3 in the reaction chamber till the surface saturation. The chamber is then purged of reactant with 300 sccm nitrogen flow for 1 second, before the introduction of the second reactant, H_2O. This second reactant oxidizes the adsorbed (MeCpPtMe3), leaving Pt on the substrate surface. After a new 2 seconds of nitrogen purge, the first step starts a new ALD cycle again. The growth rate for Pt ALD was 0.6 Å per ALD cycle.

In a final step, nanostructured manganese dioxide (MnO_2) films (several hundredth nanometer thick) are deposited by a pulsed electrodeposition method at 1.15 V vs Ag/AgCl for 100 ms and at open circuit voltage (OCV) for 1 s from a 0.1 M $MnSO_4$ / 0.1 M H_2SO_4 solution based on the optimized parameter published recently [8].

A parallel plate configuration consists in assembling two 3D electrodes in face-to-face topology where the distance between the two electrodes is fixed to 15 mm.

Fabrication of the 3D intergitated MSCs. The fabrication of 3D interdigitated MSCs is described below. The technological process (6 steps) of the MSC at the wafer level combines a top-down approach to fabricate the 3D interdigitated current collector with the bottom-up selective electroplating of MnO_2 thin films. The first stage of this process deals with the fabrication of the 3D microstructures, following a part of the process described in the previous section. Each finger of the MSC, based on an array of silicon microtubes, is separated by a silicon microribbon. A photolithography step is optimized to tune the transverse dimensions of the 3D scaffold (inner diameter = 3 µm, outer diameter = 6 µm, spacing = 3 µm) while the etching time defines the depth of the 3D scaffold[24,27]. Once the photoresist is removed from the top of the microstructures, the 2nd and 3rd step of this process are respectively the conformal deposition of an insulator layer and a current collector. 50 nm-thick insulating layer (Al_2O_3 – 1st layer) is deposited by ALD to isolate each MSC on the 3-inch silicon wafer. 50 nm-thick platinum layer (ALD - 2nd layer) acts as the current collector and the seed layer for MnO_2 electroplating deposition: this thickness is sufficient to have a continuous and highly conductive deposit. The 3D platinum layer has to be patterned (step 4) and etched (step 5). High viscosity thick photoresist is spin-coated on the 3D wafer to protect the 3D array and will be used as the etching mask of the Pt thin film.

By photolithography, a 15 µm wide spacing is opened in the photoresist on the top of the microribbon. A dry etching process (Inductively Coupled Plasma / Reactive Ion Etching) based on chlorine / argon mixture gas is used to etch the Pt (50 nm-thick) on the top of the microribbon selectively to the deposited photoresist. Once the photoresist removes from this scaffold, MnO_2 thin film is electroplated on the Si / Al_2O_3 / Pt interdigitated electrode to maximize the electrode capacitance while keeping high the power capabilities (step 6). This nanostructured MnO_2 film is deposited by pulsed electrodeposition technique with the same deposition parameters as mentioned in the previous section.

Morphological and structural analyses. The top surface and cross-section analyses of the 3D MSCs were carried out by using a ZEISS ULTRA 55 Scanning Electron Microscope (SEM). To identify the crystalline structure of the as-deposited MnO_2 thin film on Si / Al_2O_3 / Pt substrate, Raman analyses were performed with a Labram HORIBA instrument operated at λ = 471 nm UV light. There were coupled with Transmission Electron Microscopy Observations and Electron Diffraction.

Electrochemical analysis. For the testing of the 3D electrode in three electrode cell configuration, a platinum wire and an Ag/AgCl electrode were used as the counter electrode (CE) and the reference (REF) electrode, respectively. The silicon substrate with the electrode on the top was inserted in a flat cell (Bio-logic) consisting of two pieces of PTFE. The bottom part was the support for the sample and the second part was located on the top of the electrode with a gasket limiting the electrode surface to be investigated (0.45 cm^2). The two pieces were assembled with screws and a 5mm platinum coated part of the silicon substrate, not in contact with the electrolyte, served as the current collector for the working electrode. Above the electrode, a cavity was filled with the electrolyte and specific spaces were available for the

insertion of the reference and counter electrodes. The electrochemical analysis was achieved using a VMP3 potentiostat / galvanostat from Bio-Logic. Cyclic Voltamperometry (CV), Galvanostatic Charge and Discharge Cycling of the 3D electrodes and the 3D MSC were performed in 5M $LiNO_3$ aqueous electrolyte in a 1 V potential window.

To evaluate the electrochemical performance of the 3D MSCs in parallel plates configuration, two 3D MnO_2 electrodes were considered as working and counter electrodes and assembled face to face using homemade flat cell filled with 5M $LiNO_3$ aqueous electrolyte. In order to follow the electrochemical window in which each electrode was operated, the MSCs were immersed in a beaker containing the electrolyte and an Ag/AgCl reference electrode located on the top of the device allowed to control the evolution of each electrode potential. For 3D interdigitated electrodes MSCs, 100 µL of 5M $LiNO_3$ aqueous electrolyte were deposited to cover the MSCs which was inserted in a sealed box to prevent fast water evaporation.

Electrochemical Impedance Spectroscopy at the rest potential of the MSC (frequency range: 1 MHz – 20 mHz, signal amplitude = ± 25 mV) was used to evaluate the equivalent series resistance, the charge transfer resistance and to confirm the capacitive behavior of the 3D MSC.

The specific capacitance (C, $mF.cm^{-2}$), energy density (E, $\mu Wh.cm^{-2}$), and power density (P, $mW.cm^{-2}$) were evaluated according to the equations (2), (3) and (4):

$$C = \frac{\int Idt}{A\Delta V} \qquad (2)$$

$$E = \frac{C(\Delta V)^2}{2} \qquad (3)$$

$$P = 3600\frac{E}{\Delta t} \qquad (4)$$

where I is the constant charge / discharge current (mA), Δt is the charge/ discharge time, A represents the footprint area of the interdigitated MSC (16 mm^2) and ΔV is the cell voltage of the MSC (V). The cycling tests were conducted using galvanostatic charge-discharge measurements at selected current densities.

Results and discussion

Tuning the areal capacitances of pseudocapacitive electrodes with the depth of the 3D scaffold and MnO_2 thickness. The restricted available space for energy harvesting and storage sources in IoT miniaturized devices strongly limits the energy performance of micro-supercapacitors. The footprint surface of the MSC is about several tens of millimeter square. Taking into account the limited surface, the performance of the 3D MSC could be increased by one to three orders of magnitude as compared to the planar technology [7,8,24–26].

Therefore, the 3D MSC, either in parallel or interdigitated configuration, has to be carefully designed (**figure 1A)**. In particular, the evolution of the surface capacitances should be investigated with respect to the depth of the 3D scaffold and the thickness of the nanostructured MnO_2 films. It is worth pointing out that the surface capacitance (per footprint area) of the MSC is about two times greater for the parallel plate design as compared to the interdigitated topology.

The fabrication process of the 3D MnO_2 electrodes is described in the method section and is shown in **Figure S1**. This process allows to fabricate 3D MnO_2-based electrodes with very high areal capacitance values. A conformal electrodeposition of manganese dioxide film is achieved on 3D platinum-coated silicon scaffold. The films present a homogeneous aspect along the tubes with needles shape grains several tens of nanometers long (**Figures S2 and S3**). The thicknesses of the electrodeposited MnO_2 films were measured according to the top view (SEM images, **Figures S2 and S3**) of the bare microtubes and the same 3D scaffold after deposition. A structural analysis is carried out to identify the as-deposited MnO_2 polymorph. Raman Spectroscopy is a powerful tool to study the structure of MnO_2 materials thanks to its high sensitivity to amorphous and short-range order

components. Figure S4 shows the Raman spectrum of the resulting MnO_2 film. Three main features are observed at 650, 575 and 510 cm^{-1} (ν1, ν2, and ν3 respectively) and a small contribution at ν4 = 386 cm^{-1}. A small feature also appears at a wavenumber of ~ 730 cm^{-1}. According to numerous authors [29–31], these Raman characteristic bands can be assigned to a manganese oxide polymorph exhibiting a birnessite-type structure. Its layered structure is able to accommodate various types of cations in its interlayer spacing, making birnessite MnO_2 an attractive a pseudocapacitive material widely studied for electrochemical capacitor applications [18,32,33]. However, X-ray diffraction analysis did not show the presence of a crystalline phase, and electron diffraction only depicted rings instead of spots. Thus, it can be indicated that the deposited MnO_2 films are amorphous or poorly crystallized precursors of birnessite-type MnO_2. Furthermore, the average Mn oxidation state is close to 3.7, indicative of the presence of Mn(IV) and Mn(III) together with intercalated cations in the layered structure. This is in good agreement with our structural/microstructural investigations performed in our previous study [8, 23 and 40].

The **figure 1B-E** summarizes the evolution of the surface capacitance vs the depth of the 3D scaffold and the thickness of the MnO_2 film.

In the first part of this study, the thickness of the electrodeposited MnO_2 film was set to 200 nm. Three 3D scaffolds showing three different etched depths (45, 56 and 125 µm) were coated with a 200 nm-thick MnO_2 film. The corresponding Area Enhancement Factors [27] (AEF - see methods section) are 17, 22 and 47 respectively. The cyclic voltammograms in 5M $LiNO_3$ at 20 mV s^{-1} are shown in **figure 1B**. A strong enhancement of the areal capacitance was observed, moving from 75 to 185 mF cm^{-2} for 45 and 125 µm-depth, respectively, while keeping the

MnO_2 film thickness at 200 nm. The footprint surface of the 3D electrode is about 16 mm^2 (4 mm x 4 mm) while the specific surface of the deepest electrode is approximately 7.5 cm^2 (AEF = 47). As such, an enhancement of the surface capacitance was demonstrated thanks to the conformal deposition of MnO_2 film on 3D scaffolds.

The second part of the study deals with the evolution of the electrode performance with the thickness of the MnO_2 film, using a constant AEF (the etched depth) for the 3D scaffold. The results are summarized in **figure 1C-E**. Here, the geometrical dimension of the silicon microtubes were kept the same (outer diameter = 6 µm / inner diameter = 3 µm / spacing = 3 µm / depth = 99 µm / footprint surface = 16 mm^2). The corresponding AEF is 38. The same anodic pulsed electrodeposition method was used to deposit nanostructured MnO_2 films on the 3D scaffold. As depicted in **figure S2A**, optimized deposition parameters led to conformal MnO_2 films: the thickness of the MnO_2 film is uniform from the top to the bottom of the 3D microtubes scaffold. Several film thicknesses from 180 to 1240 nm (**figure S2A**) were deposited. Not surprisingly, the areal capacitances proportionally increase from 0.3 to 1.7 F cm^{-2} (measured at a scan rate of 2 mV s^{-1}) with the thickness of the MnO_2 film, **(figure 1C-D)**. Nevertheless, when the sweep rate was increased up to 100 mV s^{-1}, the areal capacitance of thicker electrodes faded down more quickly than the thinner ones (**figure 1D**). A drop of about 50 % of the initial capacitance of the 1240 nm-thick MnO_2 3D electrode was observed when the scan rate was increased from 2 to 100 mV s^{-1}. In comparison, that of thinner electrodes (180 nm) was maintained using similar electrochemical testing conditions. While the improvement of the capacitance is confirmed by increasing the thickness of MnO_2 films, this experiment also shows how the power capability of the electrode is impacted at high sweep rate for thicker

MnO_2 layer. This limit points out that the trade-off between optimum energy and power densities can be achieved by tuning the thickness of the electroactive material on the 3D scaffold.

To further investigate these behaviors, advanced electrochemical data processing such as proposed by Trasatti and co-workers [37] on RuO_2 pseudocapacitive thin film electrode was achieved. In this approach, the total capacity ($Q_{total\text{-}surface}$) of a pseudocapacitive material is said to arise from two main contributions. The first contribution originates from the sub-surface ($Q_{inner\text{-}surface}$) while the second one comes from the surface ($Q_{outer\text{-}surface}$) considering the adsorption of electrolytic species at surface redox sites as well as the diffusion towards "bulk" sites. On one hand, the areal capacity (Q^*) (in C cm^{-2}) is plotted vs of $v^{-1/2}$ for each MnO_2 thickness (180, 410, 600 and 1240 nm) (**figure S2B**). Extrapolating these plots at high scan rates ($1/v^{1/2} \rightarrow 0$) leads to the outer contribution of the capacity, $Q_{outer\text{-}surface}$. On the other hand, the reverse areal capacity ($1/Q^*$ in C^{-1} cm^2) is plotted vs of the sweep rate ($v^{1/2}$). When $v \rightarrow 0$, the capacity value corresponds to the total capacity $Q_{total\text{-}surface}$ of each 3D MnO_2 electrode (**figure S2C**). Based on these data processing, $Q_{outer\text{-}surface}$ and $Q_{total\text{-}surface}$ are plotted vs the thickness of the electrodeposited MnO_2 films (**figure 1E**). The total capacity of electrodes increase with the MnO_2-film thickness up to 600 nm while the $Q_{outer\text{-}surface}$ value tends to stabilize when the MnO_2 film is thicker than 400 nm. For thicknesses above 500-600 nm (**figure 1E**), the outer-surface capacity reaches a maximum threshold as all the $Mn^{4+}/^{3+}$ sites available at the surface of the MnO_2 deposit have been involved in a redox charge/discharge process. The total capacity is then led by the $Q_{inner\text{-}surface}$ capacity, as sub-surface $Mn^{4+/3+}$ redox centers are involved. The total capacity of the 1240 nm-thick 3D MnO_2 electrode, extracted from the Trasatti data processing method, is greater than 2 C cm^{-2}. The

corresponding total capacitance value is 2 F cm^{-2}, with regard to the 1 V wide potential window. From the CV plots, the areal capacitance is evaluated close to 1.7 F cm^{-2} for this 3D electrode, meaning that a large part of the nanostructured MnO_2 film is actually electrochemically active. This is not the case for MSCs [25,26] based on thick RuO_2 electrodes where a large amount of active material does not interact with the liquid electrolyte nor contributes to the charge storage. Nevertheless, a significant decrease of the areal capacitance was observed at high sweep rate for thicker MnO_2 layers. Based on these conclusions, a MnO_2 thickness was selected between 450 and 600 nm for further investigations.

Performance of the 3D MSC based on 3D electrodes in parallel plate configuration. Once the electrode performance regarding the depth of the 3D scaffold and the thickness of the MnO_2 films is assessed, the next main issue arises from the integration of such a 3D electrode as a part of a miniaturized electrochemical capacitor. To reach this goal, two symmetrical electrodes were fabricated on two distinct silicon wafers. Assembled in a parallel plate configuration, the resulting two-terminal 3D MSC was tested in 5M $LiNO_3$ aqueous electrolyte in a face-to-face cell configuration. The depth of the 3D scaffold was approximately 164 µm, i.e. ~ half of the thickness of the silicon wafer, while the other geometrical dimensions (inner and outer diameters, spacing) were kept as previously defined. This 3D scaffold, exhibiting an AEF close to 65, was then coated with a 50 nm-thick platinum layer deposited by Atomic Layer Deposition method followed by a 450 nm-thick nanostructured MnO_2 films deposited by the pulsed electroplating technique (**figure S4**). The electrochemical performance of this MSC (footprint surface = 4 mm x 4 mm) is shown in **figure 2**. The evolution of the surface capacitances (**figure 2B**),

deduced from the cyclic voltammetry (CV in **figure 2A**) analysis, is depicted at various sweep rates from 2 to 100 mV s^{-1}. The CVs exhibit quasi-rectangular shapes typically observed for electrochemical capacitors based on pseudocapacitive materials [38–40]. The maximum cell voltage is 1V and the areal capacitance of each electrode is 1.5 F cm^{-2}. This surface capacitance is one of the highest reported value for 3D pseudocapacitive electrodes from microfabrication technique, exceeding state of the art values [2,7,41]. The areal capacitance of the 3D MSC is 0.75 F cm^{-2} at 2 mV s^{-1} (**figure 2A-B**), half of the electrode capacitance in parallel plate configuration. At 100 mV s^{-1}, the cell capacitance remains above 0.45 F cm^{-2} which is more than half the initial capacitance. Galvanostatic Charge and Discharge curves are shown in **figure 2C** between 0 and 1 V at 0.3 mA cm^{-2} applied current density. Again, the plots exhibit a triangular shape, as expected for (pseudo)capacitive material. It was checked by using an Ag/AgCl reference electrode that each 3D electrode was operated in its safe potential window as can be seen from figure 2C. This is the guarantee for long term cycling ability. When the current density is increased up to 12.5 mA cm^{-2}, the time constant is decreased down to ~ 25 s (**figure 2D**). Overall measured capacitances perfectly fit those extracted from CV experiments. From these GCD measurements, the energy density of the MSC was evaluated vs of the current densities (**figure 2E**). The areal energy densities range from 0.1 to 0.045 mWh cm^{-2} when the current densities are increased from 0.3 up to 12.5 mA cm^{-2}. The corresponding power densities are 0.16 and 7.1 mW cm^{-2}, respectively. Since this technology is able to reach high energy density thresholds, it is critical to demonstrate the long term cycling of such fabricated 3D microdevices. The capacitance retention vs of the number of cycles operated in 5M $LiNO_3$ at 20 mV s^{-1} is depicted in **figure 2F**. After a drop of the initial capacitance (~ 15 % loss) during

the first thousand cycles, the 3D MSC exhibits a stable behavior where approximately 82 % of the initial capacitance is retained after 10 000 cycles.

Electrochemical performance of the 3D interdigitated MSC. To improve the compactness / miniaturization of the 3D MSCs, an attractive solution consists in designing 3D interdigitated MSC as depicted in **figure 1A**. This interdigitated topology allows optimizing the compactness of the microdevices but at the cost of a loss in areal energy density (see method section). For a similar footprint surface, the areal capacitance of interdigitated MSC is half that of a MSC in parallel plate configuration since the two interdigitated electrodes are in a same plane. In that configuration, the surface of each electrode corresponds approximately to half of the footprint surface of the microdevice.

The design of the 3D MSC is shown **in figure 3** where the top surface and SEM cross-sections analyses are also reported. The 3D MSC (footprint area = 1.8 mm x 2 mm, **figure 3A**) consists in two interdigitated 3D platinum based current collectors coated with MnO_2 films (**figure 3B-D**). Each finger of the current collector integrates an array of 3D silicon microtubes to improve the AEF and specific surface of the electrodes. The fabrication process is described in the methods section. According to the geometrical parameters of the 3D scaffold (outer diameter = 6 µm / inner diameter = 3 µm / spacing = 3 µm / etched depth = 125 µm), the corresponding area enhancement factor is 47. Regarding the footprint surface of the 3D MSC (1.8 mm x 2 mm), the developed surface is 1.7 cm^2 (47 x 3.6 mm^2). A nanostructured MnO_2 film (580 nm-thick) is then electrodeposited on these two interdigitated 3D current collectors (**figure 3E-F**).

Electrochemical performance of the fabricated 3D interdigitated MSC is reported in **figure 4**. To check the interdigitated electrodes are not short-circuited,

Electrochemical Impedance Spectroscopy analysis was performed on the 3D MSC in 5M $LiNO_3$. The Nyquist plot of the 3D MSC is shown in **figure 4A-B**. This plot shows the expected profile for an electrochemical capacitor based on pseudocapacitive material with a semicircle at high frequency that reflects the charge transfer process and a near vertical straight line in the low-frequency region characteristic of the capacitive behavior of the microdevice. From this plot, the time constant of the MSC was evaluated at the knee frequency (time constant ~ 17 s (f_0 = 0.058 Hz)). The equivalent series resistance (ESR) and the charge transfer resistance (R_{CT}) from the Nyquist plot are 1.5 and 6 Ω cm^2, respectively (**figure 4B**). These values are of the same order as those of obtained for other 3D MSCs [8,26].

Galvanostatic Charge Discharge (GCD) cycling plots are shown is **figure 4C** at various current densities, from 0.9 up to 15.6 mA cm^{-2}. These plots illustrate the evolution of the voltage profile of the 3D MSC between 0 and 1 V. The triangular shape of the GCD plots corresponds to the expected behavior of a MSC based on a (pseudo)capacitive material. As expected, the energy density is greater when the current density is decreased. No significant ohmic drop is observed on these GCD plots, as expected from the EIS analyses, validating the targeted film thickness and the depth of the 3D scaffold. The areal capacitance of the 3D interdigitated MSC is 0.39 F cm^{-2} at 0.9 mA cm^{-2}. Taking into account a 1 V-cell voltage, the corresponding energy and power densities are close to 0.06 mWh cm^{-2} and 0.2 mW cm^{-2}, respectively. At higher current density, the maximum power density reaches 10 mW cm^{-2} while maintaining a good energy density of 20 µWh cm^{-2}. This value, obtained at high power density, corresponds to what was obtained at lower power density by past state of the art MSCs [8,24,42], demonstrating a significant improvement of the technology. The cycling behavior of the 3D MSCs is shown in **figure 4D** where the

3D interdigitated microdevice retains 84 % of its initial capacitance after 10 000 cycles.

The performance of the two 3D MSCs are finally compared with the state of the art MSCs tested in aqueous and organic electrolytes. The results are displayed in **figure 5** where an area normalized Ragone plot of the microdevices summarize the overall performance. Whatever the configuration (parallel plate or interdigitated designs), the maximum energy density of our 3D MSCs is superior to 0.05 mWh cm^{-2}. To the author knowledge, the performance reached by the presently fabricated 3D MSCs lie among the best energy / power trade-off values of the state of the art microdevices tested in liquid electrolytes.

To reach these remarkable energy densites for compact microdevices (footprint area < 4 mm^2), many technological issues were addressed in the frame of this study. On one hand, the thickness of the nanostructured MnO_2 film is kept below 600 nm allowing to maintain a large amount of electroactive material in contact with the aqueous electrolyte and simultaneously with the 3D current collector. This is not the case for microdevices based on thick electrodes where ion and electron transport limitations occur within the electrode, giving rise to high energy density but limited rate capabilities [26,31]. Herein, the high rate capability of the 3D MSCs is demonstrated: from the Nyquist plot, a time constant close to 17 s is measured which is a typical value for EC based on pseudocapacitive material. Additionally, the conformal electrodeposition of MnO_2 films on the 3D silicon microtubes scaffold with high AEF allows maximizing the interaction between the active material and the aqueous electrolyte. On the other hand, the capacitance retention is demonstrated to be greater than 82 % over 10 000 cycles, showing the long-term durability of the microdevices and validating the enhanced robustness of the technological process.

Many recent papers do not show long term cycling and high rate capability while claiming that prepared MSCs are power microdevices with long serving life [25,26]. Finally, the fabrication process reported here is compatible with the fabrication methods issued from the semiconductor/microelectronic industry, favoring rapid scale up of the technology for mass production and shortening the time to market. Further investigations are ongoing to package the fabricated 3D microdevices with solid-state electrolytes [26,43].

Conclusion

In summary, we demonstrated the fabrication of compact 3D micro-supercapacitors (footprint area < 16 mm^2) combining thickness limited nanostructured MnO_2 films (< 600 nm) with robust 3D silicon scaffold exhibiting high area enhancement factor (x 65). The 3D strategy proposed here offers large specific surface, fast electron transport and rapid ion diffusion from the electrolyte to the redox active material. The fine tuning of 3D design and the film thickness allowed to maximize the cell capacitance (> 0.7 F cm^{-2}) and the energy density (0.05 - 1 mWh cm^{-2}) while keeping high the power density (> 1 mW cm^{-2}) and the cycling life (> 82 % of the initial capacitance after 10 000 cycles). This study gives new opportunities for designing efficient miniaturized energy storage devices and opens the road for powering the next generation of Internet of Things microdevices with robust and compact 3D micro-supercapacitors.

DATA AVALAIBILITY

The raw/processed data required to reproduce these findings cannot be shared at this time as the data also forms part of an ongoing study.

COMPETING INTERESTS.

The authors declare no competing interests.

References

[1] A. Raj, D. Steingart, Review—Power Sources for the Internet of Things, J. Electrochem. Soc. 165 (2018) B3130–B3136. doi:10.1149/2.0181808jes.

[2] C. Lethien, J. Le Bideau, T. Brousse, Challenges and prospects of 3D micro-supercapacitors for powering the internet of things, Energy Environ. Sci. 12 (2019) 96–115. doi:10.1039/C8EE02029A.

[3] P. Huang, C. Lethien, S. Pinaud, K. Brousse, R. Laloo, V. Turq, M. Respaud, A. Demortiere, B. Daffos, P.L. Taberna, B. Chaudret, Y. Gogotsi, P. Simon, On-chip and freestanding elastic carbon films for micro-supercapacitors, Science (80-.). 351 (2016) 691–695. doi:10.1126/science.aad3345.

[4] M.F. El-Kady, V. Strong, S. Dubin, R.B. Kaner, Laser Scribing of High-Performance and Flexible Graphene-Based Electrochemical Capacitors, Science (80-.). 335 (2012) 1326–1330. doi:10.1126/science.1216744.

[5] D. Pech, M. Brunet, H. Durou, P. Huang, V. Mochalin, Y. Gogotsi, P.-L. Taberna, P. Simon, Ultrahigh-power micrometre-sized supercapacitors based on onion-like carbon, Nat. Nanotechnol. 5 (2010) 651–654. doi:10.1038/nnano.2010.162.

[6] J.Y. Hwang, M.F. El-Kady, Y. Wang, L. Wang, Y. Shao, K. Marsh, J.M. Ko,

R.B. Kaner, Direct preparation and processing of graphene/RuO2 nanocomposite electrodes for high-performance capacitive energy storage, Nano Energy. 18 (2015) 57–70. doi:10.1016/j.nanoen.2015.09.009.

[7] M.F. El-Kady, M. Ihns, M. Li, J.Y. Hwang, M.F. Mousavi, L. Chaney, A.T. Lech, R.B. Kaner, Engineering three-dimensional hybrid supercapacitors and microsupercapacitors for high-performance integrated energy storage, Proc. Natl. Acad. Sci. 112 (2015) 4233–4238. doi:10.1073/pnas.1420398112.

[8] E. Eustache, C. Douard, A. Demortière, V. De Andrade, M. Brachet, J. Le Bideau, T. Brousse, C. Lethien, High Areal Energy 3D-Interdigitated Micro-Supercapacitors in Aqueous and Ionic Liquid Electrolytes, Adv. Mater. Technol. 2 (2017) 1700126. doi:10.1002/admt.201700126.

[9] K. Robert, C. Douard, A. Demortière, F. Blanchard, P. Roussel, T. Brousse, C. Lethien, On Chip Interdigitated Micro-Supercapacitors Based on Sputtered Bifunctional Vanadium Nitride Thin Films with Finely Tuned Inter- and Intracolumnar Porosities, Adv. Mater. Technol. 3 (2018) 1800036. doi:10.1002/admt.201800036.

[10] M.R. Lukatskaya, O. Mashtalir, C.E. Ren, Y. Dall'Agnese, P. Rozier, P.L. Taberna, M. Naguib, P. Simon, M.W. Barsoum, Y. Gogotsi, Cation Intercalation and High Volumetric Capacitance of Two-Dimensional Titanium Carbide, Science (80-.). 341 (2013) 1502–1505. doi:10.1126/science.1241488.

[11] M. Ghidiu, M.R. Lukatskaya, M.-Q. Zhao, Y. Gogotsi, M.W. Barsoum, Conductive two-dimensional titanium carbide 'clay' with high volumetric capacitance, Nature. 516 (2014) 78–81. doi:10.1038/nature13970.

[12] B. Anasori, M.R. Lukatskaya, Y. Gogotsi, 2D metal carbides and nitrides

(MXenes) for energy storage, Nat. Rev. Mater. 2 (2017) 16098. doi:10.1038/natrevmats.2016.98.

[13] D. Choi, G.E. Blomgren, P.N. Kumta, Fast and reversible surface redox reaction in nanocrystalline vanadium nitride supercapacitors, Adv. Mater. 18 (2006) 1178–1182. doi:10.1002/adma.200502471.

[14] T.-C. Liu, W.G. Pell, S.L. Roberson, B.E. Conway, Behavior of Molybdenum Nitrides as Materials for Electrochemical Capacitors, J. Electrochem. Soc. 145 (1998) 1882. doi:10.1149/1.1838571.

[15] Y. Borjon-Piron, A. Morel, D. Bélanger, R.L. Porto, T. Brousse, Suitable Conditions for the Use of Vanadium Nitride as an Electrode for Electrochemical Capacitor, J. Electrochem. Soc. 163 (2016) A1077–A1082. doi:10.1149/2.1221606jes.

[16] K. Robert, D. Stiévenard, D. Deresmes, C. Douard, A. Iadecola, D. Troadec, P. Simon, N. Nuns, M. Marinova, M. Huvé, P. Roussel, T. Brousse, C. Lethien, Novel insights into the charge storage mechanism in pseudocapacitive vanadium nitride thick films for high-performance on-chip micro-supercapacitors, Energy Environ. Sci. 13 (2020) 949–957. doi:10.1039/c9ee03787j.

[17] B.E. Conway, The Electrochemical Behavior of Ruthenium Oxide (RuO2) as a Material for Electrochemical Capacitors, in: Electrochem. Supercapacitors, 1999: pp. 259–297. doi:10.1007/978-1-4757-3058-6_11.

[18] M. Toupin, T. Brousse, D. Bélanger, Influence of microstucture on the charge storage properties of chemically synthesized manganese dioxide, Chem. Mater. 14 (2002) 3946–3952. doi:10.1021/cm020408q.

[19] V. Augustyn, J. Come, M.A. Lowe, J.W. Kim, P.-L. Taberna, S.H. Tolbert, H.D. Abruña, P. Simon, B. Dunn, High-rate electrochemical energy storage through Li+ intercalation pseudocapacitance, Nat. Mater. 12 (2013) 518–522. doi:10.1038/nmat3601.

[20] C. Arico, S. Ouendi, P.-L. Taberna, P. Roussel, P. Simon, C. Lethien, Fast Electrochemical Storage Process in Sputtered Nb2O5 Porous Thin Films, ACS Nano. 13 (2019) 5826–5832. doi:10.1021/acsnano.9b01457.

[21] J.-L. Codron, S. Ouendi, P. Simon, P. Roussel, C. Lethien, C. Arico, L. Clavier, X. Wallart, F. Blanchard, P.L. Taberna, Synthesis of T-Nb2O5 thin-films deposited by Atomic Layer Deposition for miniaturized electrochemical energy storage devices, Energy Storage Mater. 16 (2018) 581–588. doi:10.1016/j.ensm.2018.08.022.

[22] H. Durou, D. Pech, D. Colin, P. Simon, P.-L. Taberna, M. Brunet, Wafer-level fabrication process for fully encapsulated micro-supercapacitors with high specific energy, Microsyst. Technol. 18 (2012) 467–473. doi:10.1007/s00542-011-1415-7.

[23] F. Li, M. Huang, J. Wang, J. Qu, Y. Li, L. Liu, V.K. Bandari, Y. Hong, B. Sun, M. Zhu, F. Zhu, Y.X. Zhang, O.G. Schmidt, On-chip 3D interdigital micro-supercapacitors with ultrahigh areal energy density, Energy Storage Mater. 27 (2020) 17–24. doi:10.1016/j.ensm.2020.01.008.

[24] E. Eustache, C. Douard, R. Retoux, C. Lethien, T. Brousse, MnO2 Thin Films on 3D Scaffold: Microsupercapacitor Electrodes Competing with “bulk” Carbon Electrodes, Adv. Energy Mater. 5 (2015) 3–7. doi:10.1002/aenm.201500680.

[25] A. Ferris, S. Garbarino, D. Guay, D. Pech, 3D RuO2 Microsupercapacitors with

Remarkable Areal Energy, Adv. Mater. 27 (2015) 6625–6629. doi:10.1002/adma.201503054.

[26] A. Ferris, D. Bourrier, S. Garbarino, D. Guay, D. Pech, 3D Interdigitated Microsupercapacitors with Record Areal Cell Capacitance, Small. 15 (2019) 1–8. doi:10.1002/smll.201901224.

[27] E. Eustache, P. Tilmant, L. Morgenroth, P. Roussel, G. Patriarche, D. Troadec, N. Rolland, T. Brousse, C. Lethien, Silicon-microtube scaffold decorated with anatase TiO2 as a negative electrode for a 3D litium-ion microbattery, Adv. Energy Mater. 4 (2014) 1–11. doi:10.1002/aenm.201301612.

[28] J. Le Bideau, F. Thissandier, P. Gentile, T. Brousse, S. Sadki, M. Brachet, G. Bidan, N. Berton, Wide-voltage-window silicon nanowire electrodes for micro-supercapacitors via electrochemical surface oxidation in ionic liquid electrolyte, Electrochem. Commun. 41 (2014) 31–34. doi:10.1016/j.elecom.2014.01.010.

[29] H.A. Mosqueda, O. Crosnier, L. Athouël, Y. Dandeville, Y. Scudeller, P. Guillemet, D.M. Schleich, T. Brousse, Electrolytes for hybrid carbon–MnO2 electrochemical capacitors, Electrochim. Acta. 55 (2010) 7479–7483. doi:https://doi.org/10.1016/j.electacta.2010.01.022.

[30] J. Jiang, B. Liu, G. Liu, D. Qian, C. Yang, J. Li, A systematically comparative study on LiNO3 and Li2SO4 aqueous electrolytes for electrochemical double-layer capacitors, Electrochim. Acta. 274 (2018) 121–130. doi:https://doi.org/10.1016/j.electacta.2018.04.097.

[31] P. Zhang, Y. Li, G. Wang, F. Wang, S. Yang, F. Zhu, X. Zhuang, O.G. Schmidt, X. Feng, Zn-Ion Hybrid Micro-Supercapacitors with Ultrahigh Areal Energy Density and Long-Term Durability, Adv. Mater. 31 (2019) 1–6.

doi:10.1002/adma.201806005.

[32] C. Julien, M. Massot, R. Baddour-hadjean, S. Franger, S. Bach, J.P. Pereira-ramos, Raman spectra of birnessite manganese dioxides, Solid State Ionics. 159 (2003) 345–356. doi:10.1016/S0167-2738(03)00035-3.

[33] C. Julien, M. Massot, S. Rangan, M. Lemal, D. Guyomard, Study of structural defects in g -MnO 2 by Raman spectroscopy, J. Raman Spectrosc. 33 (2002) 223–228. doi:10.1002/jrs.838.

[34] D. Chen, D. Ding, X. Li, G.H. Waller, X. Xiong, M.A. El-Sayed, M. Liu, Probing the Charge Storage Mechanism of a Pseudocapacitive MnO 2 Electrode Using in Operando Raman Spectroscopy, Chem. Mater. 27 (2015) 6608–6819. doi:10.1021/acs.chemmater.5b03118.

[35] M. Toupin, T. Brousse, D. Bélanger, Charge storage mechanism of MnO2 electrode used in aqueous electrochemical capacitor, Chem. Mater. 16 (2004) 3184–3190. doi:10.1021/cm049649j.

[36] O. Ghodbane, J. Pascal, F. Favier, Microstructural Effects on Charge-Storage Properties in MnO 2 -Based Electrochemical, ACS Appl. Mater. Interfaces. 1 (2009) 1130–1135. doi:10.1021/am900094e.

[37] S. Ardizzone, G. Fregonara, S. Trasatti, “Inner” and “outer” active surface of RuO2 electrodes, Electrochim. Acta. 35 (1990) 263–267. doi:10.1016/0013-4686(90)85068-X.

[38] T. Brousse, D. Bélanger, J.W. Long, To Be or Not To Be Pseudocapacitive?, J. Electrochem. Soc. 162 (2015) A5185–A5189. doi:10.1149/2.0201505jes.

[39] P. Simon, Y. Gogotsi, Materials for electrochemical capacitors, Nat. Mater. 7

(2008) 845–854. doi:10.1038/nmat2297.

[40] M.R. Lukatskaya, B. Dunn, Y. Gogotsi, Multidimensional materials and device architectures for future hybrid energy storage, Nat. Commun. 7 (2016) 12647. doi:10.1038/ncomms12647.

[41] T.M. Dinh, A. Achour, S. Vizireanu, G. Dinescu, L. Nistor, K. Armstrong, D. Guay, D. Pech, Hydrous RuO2/carbon nanowalls hierarchical structures for all-solid-state ultrahigh-energy-density micro-supercapacitors, Nano Energy. 10 (2014) 288–294. doi:10.1016/j.nanoen.2014.10.003.

[42] D. Pech, M. Brunet, H. Durou, P. Huang, V. Mochalin, Y. Gogotsi, P.-L. Taberna, P. Simon, Ultrahigh-power micrometre-sized supercapacitors based on onion-like carbon, Nat. Nanotechnol. 5 (2010) 651–654. doi:10.1038/nnano.2010.162.

[43] B. Asbani, B. Bounor, K. Robert, C. Douard, L. Athouël, C. Lethien, J. Le Bideau, T. Brousse, Reflow Soldering-Resistant Solid-State 3D Micro-Supercapacitors Based on Ionogel Electrolyte for Powering the Internet of Things, J. Electrochem. Soc. 167 (2020) 100551–100559. doi:10.1149/1945-7111/ab9ccc.

List of the figures and figures captions

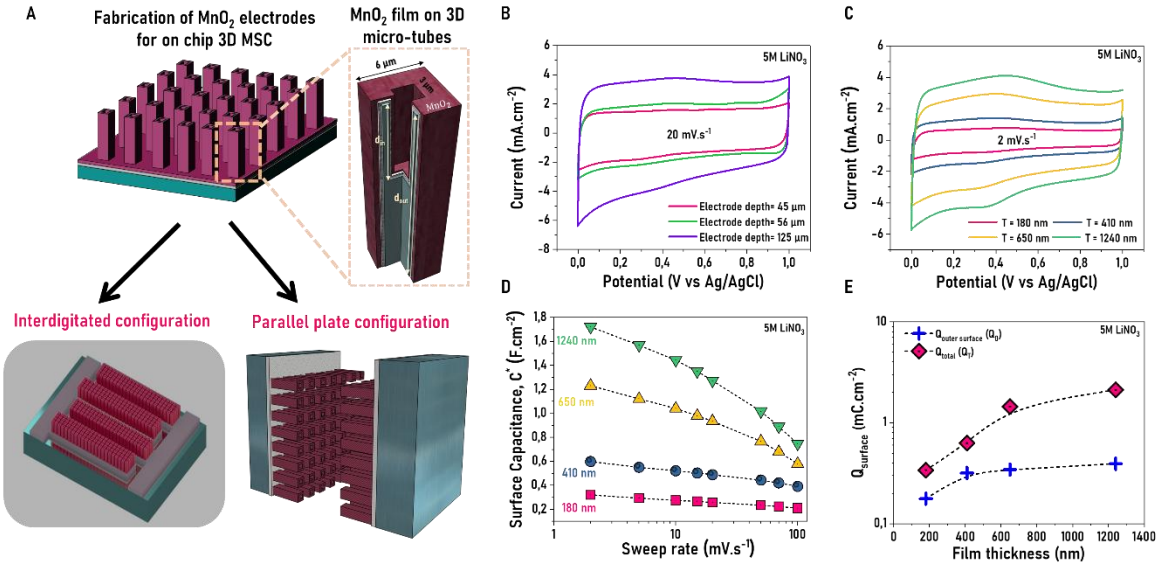

Fig. 1 | A. Overview of the strategy used to produce high performance on chip micro-supercapacitors: the interdigitated and parallel plate configurations of 3D MSC based on Si microtubes scaffold are illustrated. A zoom of an individual microtube coated with Pt / MnO_2 thin films is presented. **B.** CV at 20 mV s^{-1} in 5M $LiNO_3$ aqueous electrolyte of three different 3D electrodes vs*vs* the etched depth. For each depth (45, 56 and 125 µm respectively), the electrode was coated with 200 nm-thick MnO_2 film. **C.** CV of 3D electrodes vs*vs* of the film thickness. For each MnO_2 thickness, the geometrical parameters of the Si microtubes scaffold are fixed (outer diameter = 6 µm, inner diameter = 3 µm, depth = 100 µm). **D.** Evolution of the areal capacitance vs the film thickness at different sweep rates from 2 to 100 mV s^{-1}. **E.** Evolution of the outer-surface (Q_O) and total-surface capacity (Q_T) values vs the MnO_2 film thickness.

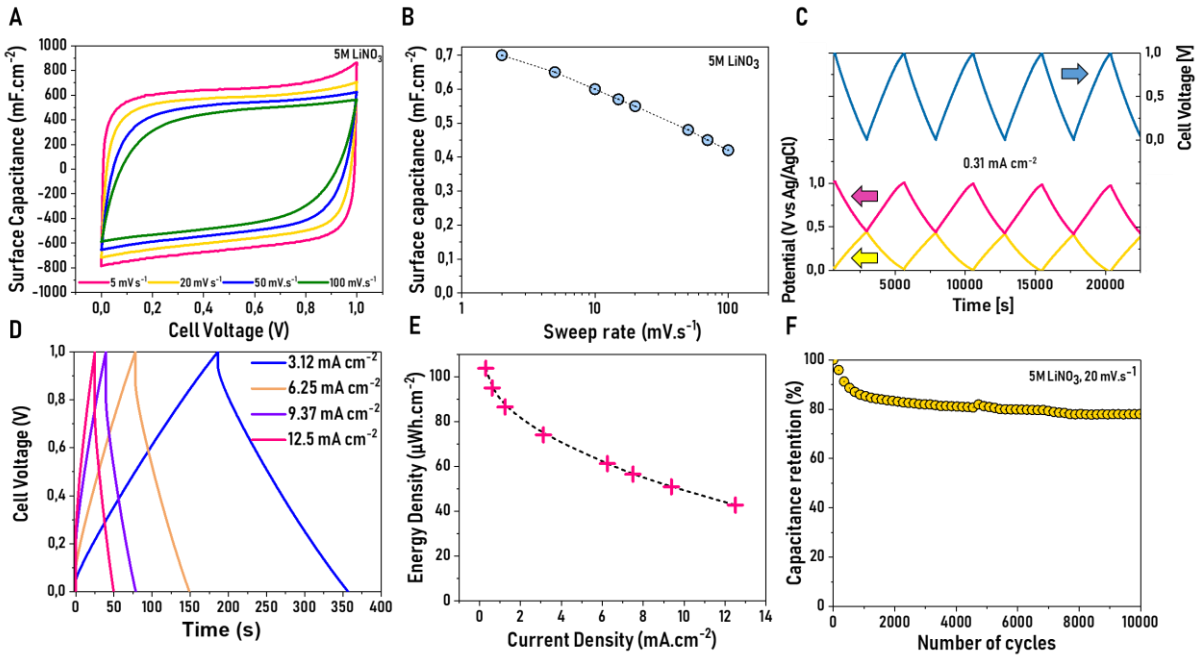

Fig. 2 | **A.** Cyclic voltammetry of a 3D MSC in parallel plate configuration measured in 5M $LiNO_3$ vs of the sweep rate. For this MSC, a surface enhancement factor of 65 is evaluated while the MnO_2 film thickness is kept constant to 450 nm. **B.** Evolution of the surface capacitance of the MSC vs the sweep rate. **C.** Galvanostatic charge and discharge (GCD) profile of the MSC (cell voltage = 1 V) at 0.31 mA cm^{-2} current density. The potential of each electrode (pink and yellow curves) and the cell voltage (blue curve) are illustrated on this plot. **D.** GCD plots vs of the current densities (3.12, 6.25, 9.37 and 12.5 mA cm^{-2} respectively). **E.** Areal Energy density of the MSC vs of the current density. **F.** Evolution of the capacitance retention vs of the number of cycles at 20 mV s^{-1}.

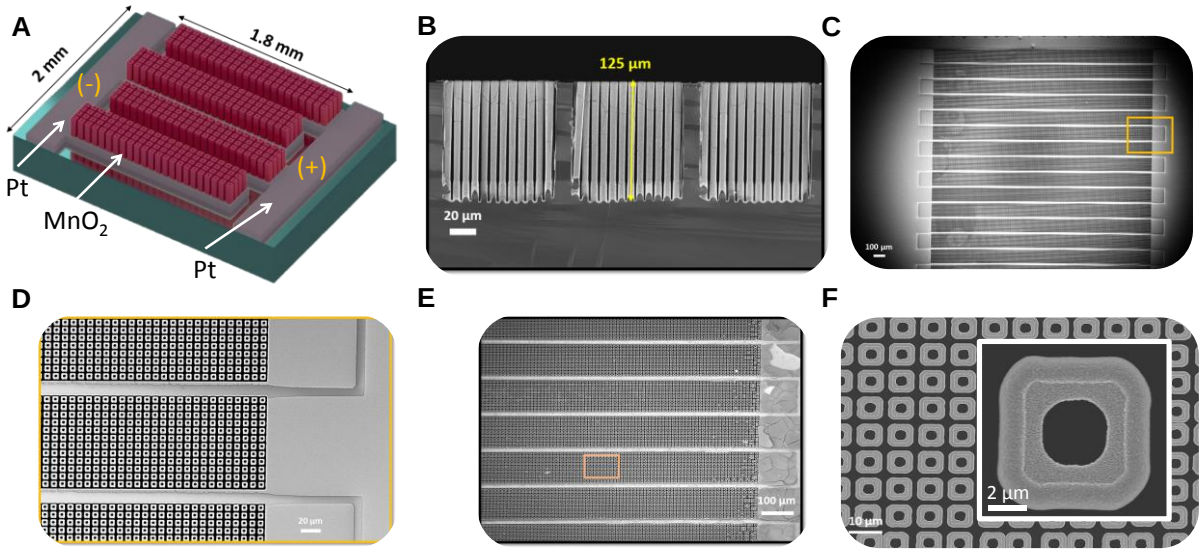

Fig. 3 | 3D interdigitated MSC. **A.** Sketch up of the 3D interdigitated MSC. **B.** SEM cross-section analyses of the MSC highlighting the etched depth of the silicon microtubes scaffold (125 µm). Top view SEM images of the 3D MSC before (**C-D**) and after deposition of the MnO_2 film (**E-F**).

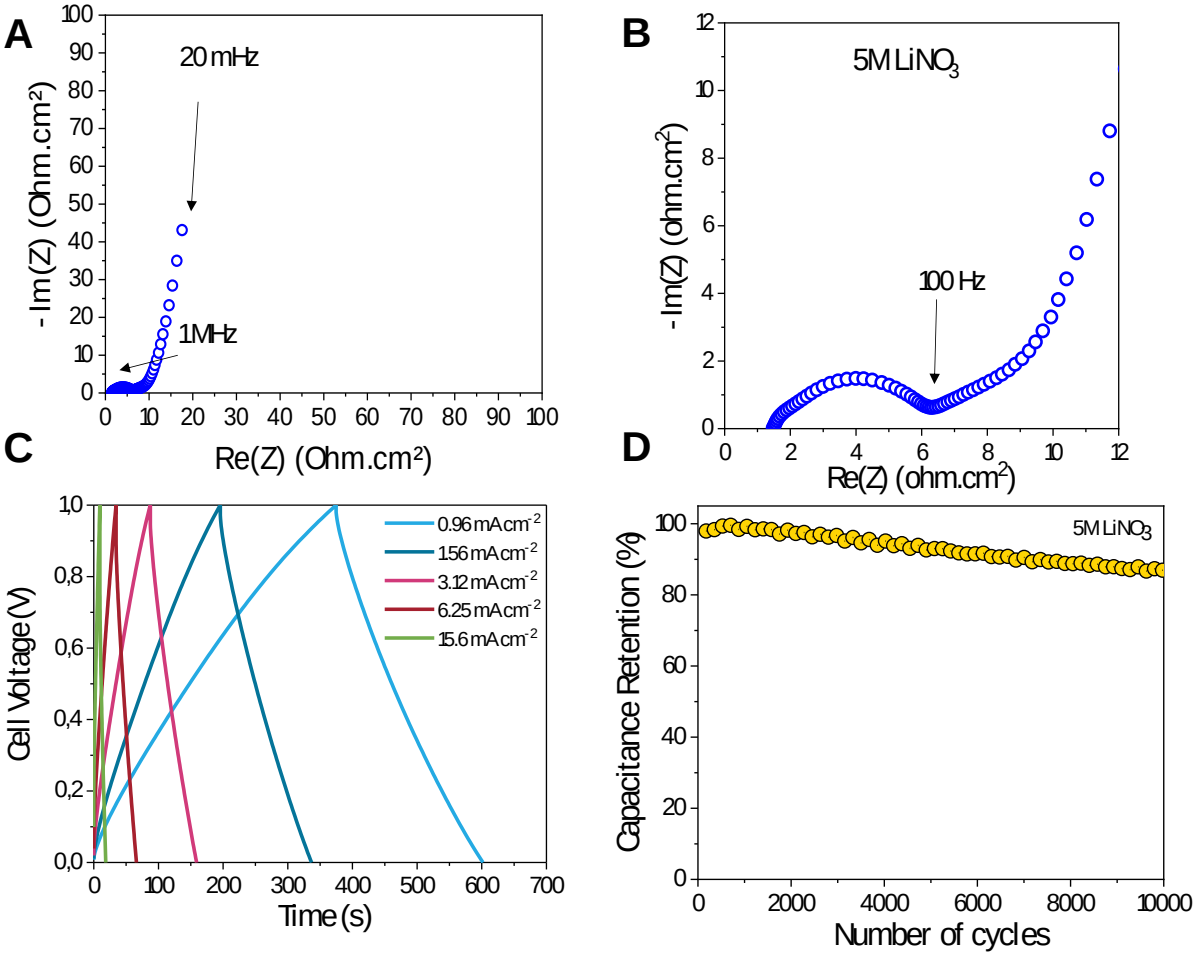

Fig. 4 | Performance of the interdigitated MSC. **A-B.** Nyquist plots of the MSC based on interdigitated topology tested in 5M $LiNO_3$. **C.** GCD profile of the MSC at different current densities. **D.** Evolution the capacitance retention vs the number of cycles at 3.1 mA cm^{-2}.

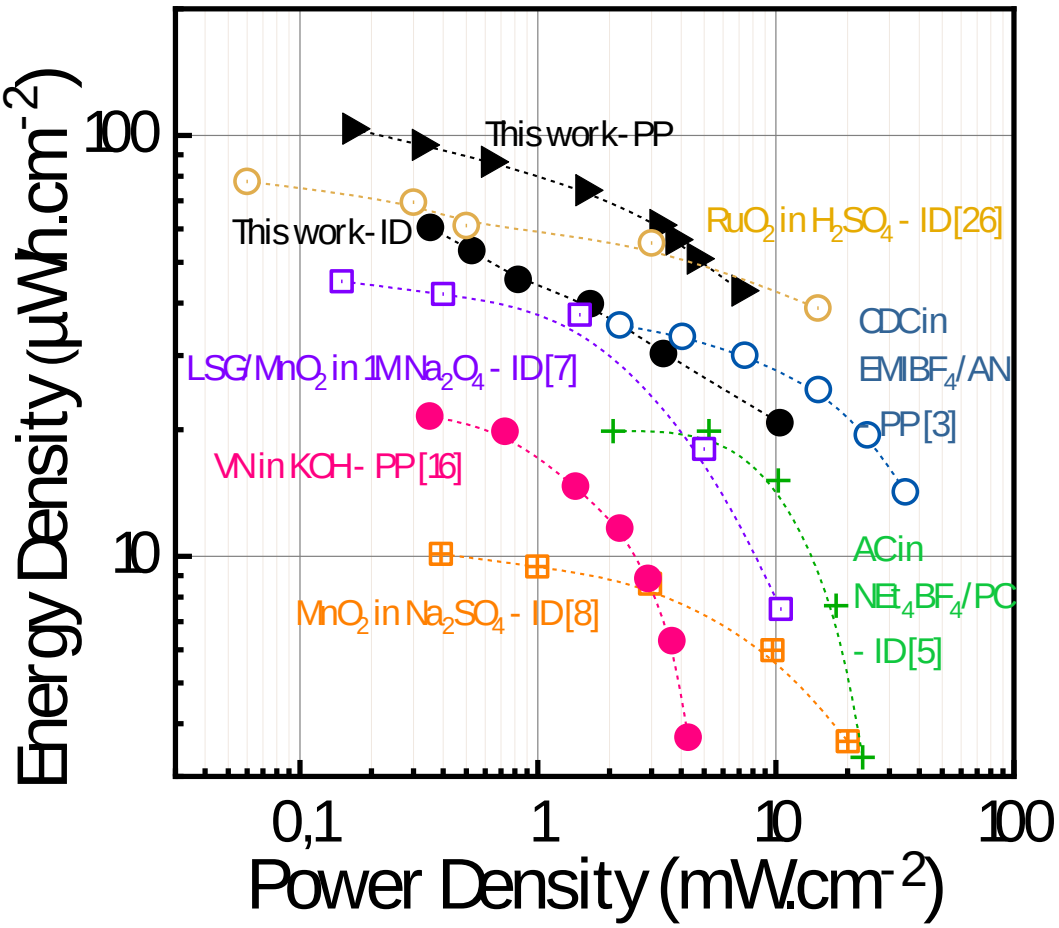

Fig. 5 | Ragone plot comparing the energy and power density per footprint area of the 3D MSCs based on parallel plate or interdigitated topologies vs the state-of-the-art MSCs.

Supplementary information

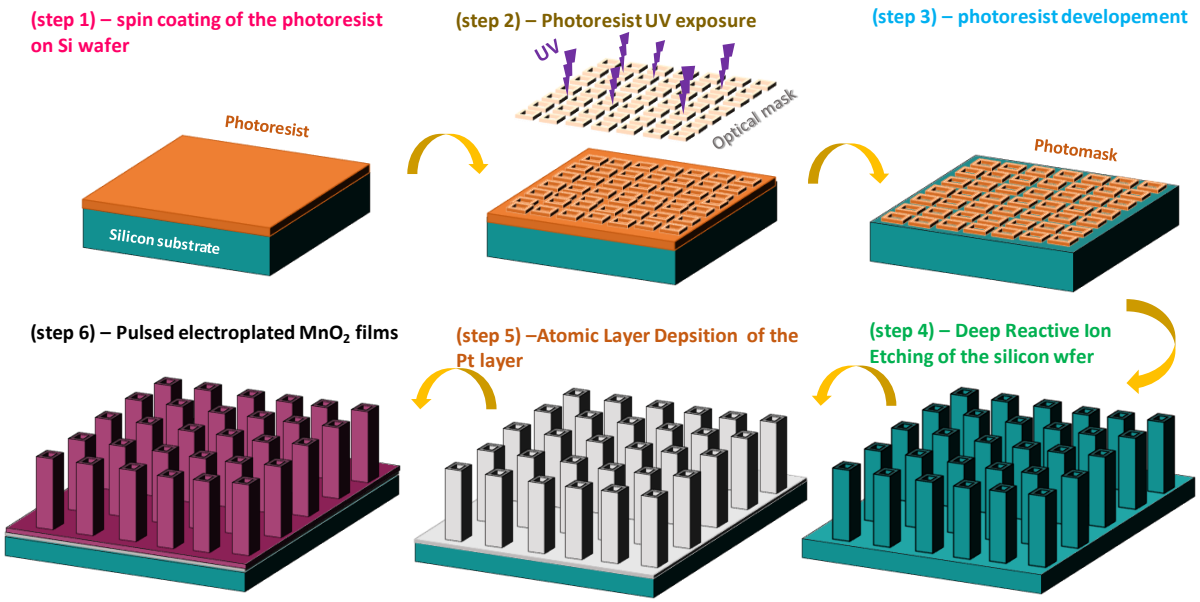

Fig. S1 | Overview of the technological fabrication process (6 steps) used to prepare the 3D electrodes of the micro-supercapacitor.

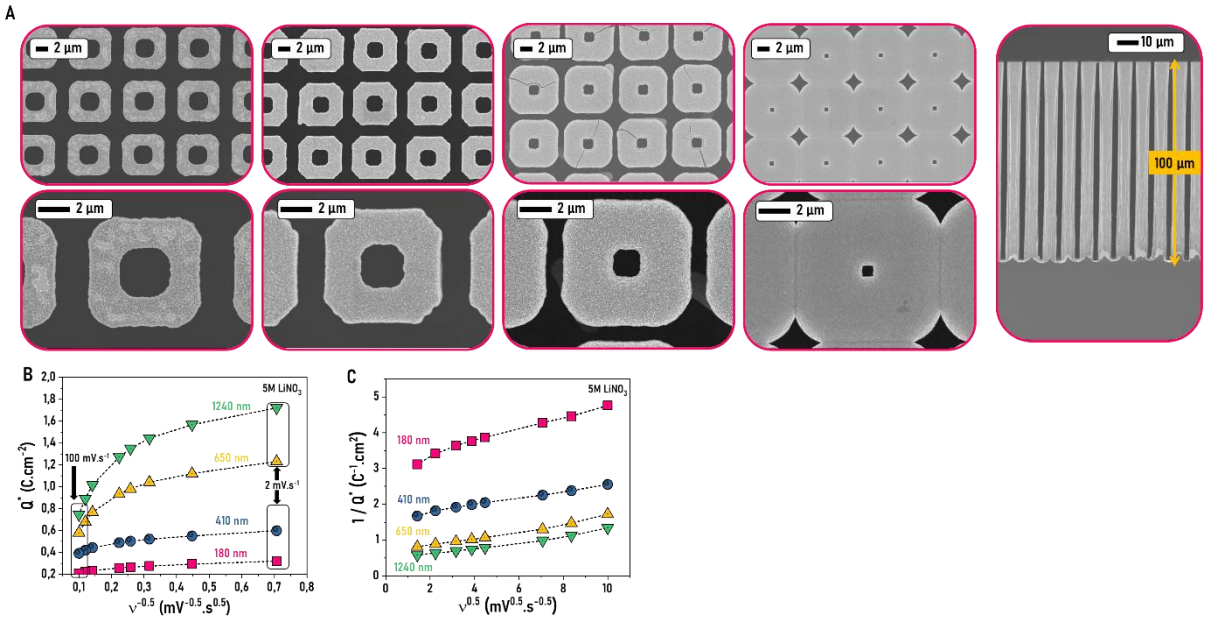

Fig. S2 | A. SEM images of thick MnO_2 film deposited on 3D silicon microtubes scaffold, from 180 nm-thick up to 1240 nm-thick (top view and cross section images). **B.** Evolution of the $Q_{surface}$ vs $\nu^{-0.5}$. **C.** Evolution of the 1 / $Q_{surface}$ vs $\nu^{0.5}$.

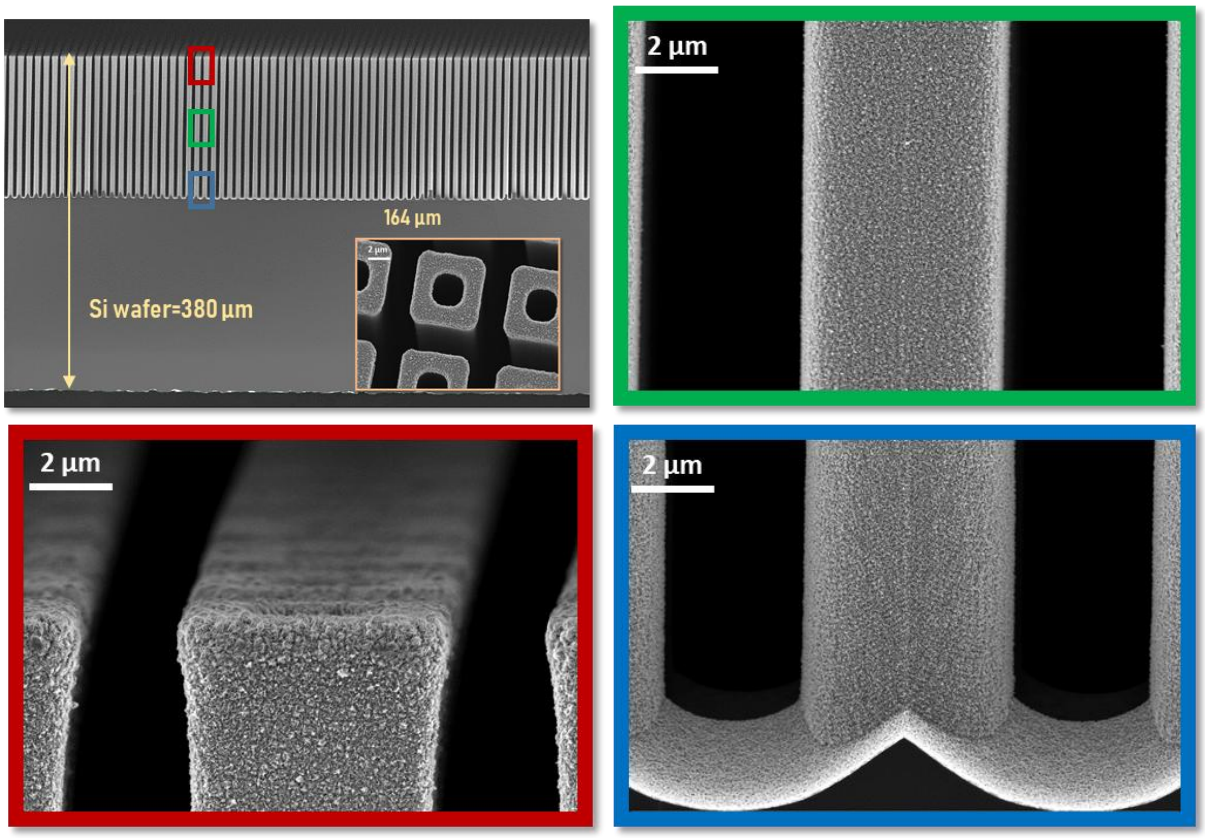

Fig. S3 | SEM images of MnO_2 film (450 nm-thick) deposited on 3D silicon microtubes scaffold (164 µm-depth / AEF = 65). The Illustration of the conformal deposited Pt / MnO_2 stacked layers on one Si microtubes, from the top to the bottom is reported.

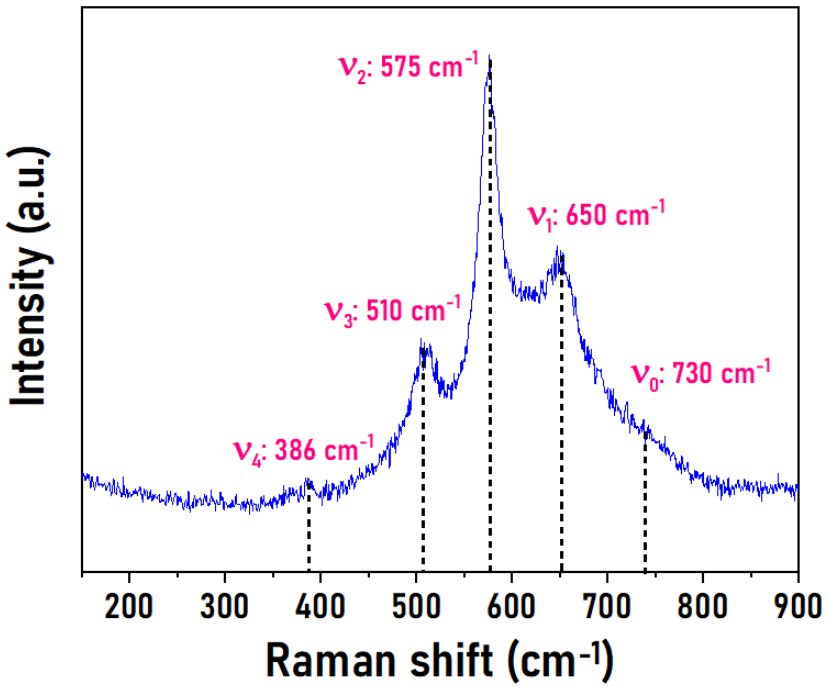

Fig. S4 | Raman spectroscopy analysis of the electrodeposited MnO_2 films on Si / Al_2O_3 / Pt substrate.